Mon. Not. R. Astron. Soc. **000**, 1–10 (xxx) Printed 18 January 2016 (MN LATEX style file v2.2)

Matter Perturbations in Scaling Cosmology

A. Romero Fuño,[1⋆] W.S. Hipólito-Ricaldi,[2] † and W. Zimdahl,[1] ‡
[1] *Universidade Federal do Espírito Santo, Departamento de Física, Av. Fernando Ferrari, 514, Campus de Goiabeiras, CEP 29075-910, Vitória, Espírito Santo, Brazil*
[2] *Universidade Federal do Espírito Santo, Departamento de Ciências Naturais, Rodovia BR 101 Norte, km. 60, Campus de São Mateus, CEP 29932-540, São Mateus, Espírito Santo, Brazil*

arXiv:1409.7706v2 [astro-ph.CO] 15 Jan 2016

xxxx. xxxx; xxx

ABSTRACT
A suitable nonlinear interaction between dark matter with an energy density ρ_M and dark energy with an energy density ρ_X is known to give rise to a non-canonical scaling $\rho_M \propto \rho_X a^{-\xi}$ where ξ is a parameter which generally deviates from $\xi = 3$. Here we present a covariant generalization of this class of models and investigate the corresponding perturbation dynamics. The resulting matter power spectrum for the special case of a time-varying Lambda model is compared with data from the SDSS DR9 catalogue. We find a best-fit value of $\xi = 3.25$ which corresponds to a decay of dark matter into the cosmological term. Our results are compatible with the ΛCDM model at the 2σ confidence level.

Key words: cosmology: dark energy – cosmology: dark matter.

1 INTRODUCTION

The currently preferred cosmological model, the ΛCDM model, is characterized by a pressureless dark-matter (DM) component with an energy density ρ_M, which decays with the third power of the cosmic scale factor a and a constant energy density ρ_Λ, attributed to a cosmological constant Λ. Alternative models, as far as they remain in the context of Friedmann-Lemaître-Robertson-Walker (FLRW) models, replace ρ_Λ by a (not necessarily constant) ρ_X, the energy density of dark energy (DE), equipped with an equation-of-state (EoS) parameter w which may be time dependent. Together, DM and DE form a "dark sector" which makes up about 95% of the present cosmic energy budget and which therefore dominates the cosmological dynamics. In the simplest case, following the ΛCDM paradigm, DM and DE are considered to be independent entities, governed by separate conservation laws. The more general case is, however, not to exclude the possibility of a non-gravitational coupling between these both components which results in a richer structure of the dark sector. Moreover, it has been demonstrated, that ignoring a potentially existing interaction may lead to an incorrect interpretation of cosmological observations (Park et al. 2009). Since neither the physical nature of DE nor that of DM are known, these models are necessarily phenomenological. Since they differ from the standard ΛCDM model they are useful to test potential deviations from the latter. While for the homogeneous and isotropic background dynamics a lot of models do fit the observations, their different perturbation dynamics may serve to limit the number of seriously competing approaches. There exists a large body of literature in which non-gravitational interactions between DE and DM are considered. A subclass of these activities is devoted to models of DE which keep an EoS parameter $w = -1$ as in the standard model, but generalize the latter insofar as ρ_X is admitted to be time dependent. These models are also called decaying Λ models (Özer & Taha 1986, 1987; Bertolami 1986; Freese et al. 1987; Chen & Wu 1990; Berman 1991; Carvalho, Lima & Waga 1992; Arbab & Abdel-Rahman 1994; Lima & Trodden 1996; Overduin & Cooperstock 1998; Overduin 1999; John & Joseph 2000; Bertolami & Martins 2000; Vishwakarma 2001; Al-Rawaf 2001; Mak, Belinchón & Harko 2002; Mboyne 2003; Alcaniz & Maia 2003; Shapiro et al. 2003; Cunha & Santos 2004; Opher & Pelinson 2004; Horvat 2004; Wang & Meng 2004; Shapiro, Solà & Štefančic 2005; Elizalde et al. 2005; Aldrovandi, Beltrán Almeida & Pereira 2005; Bauer 2005; Wang, Gong & Abdalla 2005; Barrow & Clifton 2006; Wang, Lin & Abdalla 2006; Montenegro Jr & Carneiro 2007). Our aim here is to study in this context the perturbation dynamics of a model in which DM and DE interact in such a way that the ratio of their energy densities obeys a power-law in the scale factor, i.e. $\rho_M/\rho_X \propto a^{-\xi}$, where ξ is a constant parameter. Such model was proposed by Dalal et al. (Dalal et al. 2001) to address the coincidence problem. Independently of whether or not one considers this problem to be really a problem, the ansatz by Dalal et al. gives rise to a testable alternative cosmological dynamics which

⋆ E-mail: alonsoromero.ufes@gmail.com
† E-mail: wiliam.ricaldi@ufes.br
‡ E-mail: winfried.zimdahl@pq.cnpq.br

contains the standard model as a limiting case. Various aspects of the background dynamics of this model have been studied so far and were confronted with observational data (Zimdahl & Pavón 2003; Pavón, Sen & Zimdahl 2004; Chen et al. 2010; Castro et al. 2012). This model is different from most other interacting models insofar as the interaction term is proportional to the product of the energy densities of DE and DM, i.e., the interaction is nonlinear. Most approaches in the literature deal with an interaction linear in the energy density of one of the components (see, e.g., Gavela et al. (2010); Pettorino (2013); Salvatelli et al. (2013). But in its original form its validity is restricted to the homogeneous and isotropic background. The dynamics depends directly on the scale factor which is not a covariant quantity. Here we present a covariant generalization of this model and complement previous investigations by a gauge-invariant perturbation analysis. To this purpose the scale factor is replaced by a general, covariantly defined length scale which under the conditions of homogeneity and isotropy reduces to the scale factor. This allows us to establish a covariant and gauge-invariant perturbation theory on the basis of which we calculate the matter power spectrum and discuss its dependence on the parameter ξ.

The paper is organized as follows. In Sec. 2 we present the basic framework for an interacting system of two perfect fluids. Our scaling model is established in Sec. 3 where we also study its dynamics in the spatially homogeneous and isotropic background. The perturbation analysis is the subject of Sec. 4. It provides us with an expression for the matter-density perturbation which is analyzed and observationally tested in Sec. 5. A summary of the paper is given in Sec. 6.

2 INTERACTING TWO-COMPONENT SYSTEM

We assume the cosmic substratum to be dynamically dominated by a dark sector, made of DM and DE. The substratum as a whole is characterized by a conserved total perfect-fluid type energy-momentum tensor $T_{ik} = \rho u_i u_k + p h_{ik}$ with $T^{ik}_{\ ;k} = 0$. Here, $h_{ik} = g_{ik} + u_i u_k$ and $g_{ik}u^i u^k = -1$. The quantity u^i is the total four-velocity of the cosmic substratum and latin indices run from 0 to 3. Splitting the conservation laws into their timelike and spacelike parts, we have

$$\rho_{,a}u^a + \Theta\,(\rho + p) = 0 \quad \text{and} \quad (\rho + p)\,\dot{u}^a + p_{,i}h^{ai} = 0\,, \qquad (1)$$

respectively, where $\Theta \equiv u^a_{\ ;a}$. Now we assume a split of T_{ik} into a matter component (subindex M) and a dark energy component (subindex X), according to $T^{ik} = T^{ik}_M + T^{ik}_X$ with $(A = M, X)$

$$T^{ik}_A = \rho_A u^i_A u^k_A + p_A h^{ik}_A\,, \qquad h^{ik}_A = g^{ik} + u^i_A u^k_A\,. \qquad (2)$$

An interaction between the components is covariantly characterized by

$$T^{ik}_{M\ ;k} = Q^i, \qquad T^{ik}_{X\ ;k} = -Q^i\,. \qquad (3)$$

Then, the separate energy-balance equations are

$$-u_{Mi}T^{ik}_{M\ ;k} = \rho_{M,a}u^a_M + \Theta_M\,(\rho_M + p_M) = -u_{Ma}Q^a \qquad (4)$$

and

$$-u_{Xi}T^{ik}_{X\ ;k} = \rho_{X,a}u^a_X + \Theta_X\,(\rho_X + p_X) = u_{Xa}Q^a\,. \qquad (5)$$

The four-velocities, in general different for both components, obey $g_{ik}u^i_A u^k_A = -1$. The quantities Θ_A are $\Theta_A \equiv u^a_{A;a}$. In the homogeneous and isotropic background we assume all four-velocities to coincide: $u^a_M = u^a_X = u^a$. The coupled momentum balances are

$$h^a_{Mi}T^{ik}_{M\ ;k} = (\rho_M + p_M)\,\dot{u}^a_M + p_{M,i}h^{ai}_M = h^a_{Mi}Q^i \qquad (6)$$

and

$$h^a_{Xi}T^{ik}_{X\ ;k} = (\rho_X + p_X)\,\dot{u}^a_X + p_{X,i}h^{ai}_X = -h^a_{Xi}Q^i\,, \qquad (7)$$

where $\dot{u}^a_A \equiv u^a_{A;b}u^b_A$.

It is convenient to decompose the source term Q^i into parts proportional and perpendicular to the total four-velocity,

$$Q^i = u^i Q + \bar{Q}^i\,, \qquad (8)$$

where $Q \equiv -u_i Q^i$ and $\bar{Q}^i \equiv h^i_a Q^a$ with $u_i\bar{Q}^i = 0$.

3 THE MODEL AND ITS BACKGROUND DYNAMICS

3.1 The model

Following Ellis (2009), we introduce a covariant length scale l by

$$\frac{\dot{l}}{l} \equiv \frac{1}{3}\Theta\,, \qquad \dot{l} \equiv l_{,a}u^a\,. \qquad (9)$$

Our aim is to consider the dynamics of a class of models for which the ratio of the energy densities of both components, $r \equiv \frac{\rho_M}{\rho_X}$, behaves as a power of the length scale l,

$$r = \frac{\rho_M}{\rho_X} \quad \Rightarrow \quad r = r_0 l^{-\xi}\,, \qquad (10)$$

where ξ is a constant parameter and r_0 is the present value of the ratio r. The evolution of the ratio r is then given

$$\frac{\dot{r}}{r} \equiv \frac{r_{,a}u^a}{r} = -\frac{\xi}{3}\Theta\,. \qquad (11)$$

Only tensorial quantities were used here. Relations (9), (10) and (11) generalize a previous model introduced by Dalal et al. (2001) which subsequently was studied in detail in Zimdahl & Pavón (2003); Chen et al. (2010); Castro et al. (2012); Pavón, Sen & Zimdahl (2004). In its original form, this model was restricted to the homogeneous and isotropic background dynamics. Our covariant generalization relying on the use of the length scale (9) opens the possibility to consider an inhomogeneous perturbation dynamics as well. In the background one has $\Theta = 3H = 3\frac{\dot{a}}{a}$, were a is the scale factor of the Robertson-Walker metric and (10) reduces to $r = r_0 a^{-\xi}$ which defines the class of models considered in Dalal et al. (2001).

3.2 Background dynamics

Assuming a pressureless matter component, in the homogeneous and isotropic background the balance equations (4) and (5) reduce to

$$\dot{\rho}_M + 3H\rho_M = Q \quad \text{and} \quad \dot{\rho}_X + 3H(1+w)\rho_X = -Q\,, \qquad (12)$$

respectively, where $w \equiv \frac{p_X}{\rho_X}$ is the EoS parameter of the DE and Q is the background value of the general source term Q. Combining the background ansatz $r = r_0 a^{-\xi} \Rightarrow \dot{r} = -\xi H r$ with the balances (12) yields

$$Q = -3H\left(\frac{\xi}{3} + w\right)\frac{\rho_M \rho_X}{\rho} = -3H\rho_M \frac{\frac{\xi}{3} + w}{r_0 a^{-\xi} + 1}. \tag{13}$$

This relation determines the interaction that is necessary to generate a dynamics with $r = r_0 a^{-\xi}$. The interaction vanishes for the special cases $\xi = -3w$. The ΛCDM model is recovered for $\xi = 3$ and $w = -1$. Every combination $\frac{\xi}{3} + w \neq 0$ gives rise to an alternative, testable model.

It is worth noting that we are not starting with a phenomenological ansatz for a potential interaction and then study the resulting dynamics. Rather we assume a specific dynamics, the power-law behavior $r = r_0 a^{-\xi}$ with the ΛCDM dynamics as well-defined special case, and then find the coupling that is necessary to produce such behavior.

We emphasize that the interaction (13) is a nonlinear interaction. It depends on the product of the densities of the interacting components. This makes it different from and obviously more "realistic" than most of the other interactions between DM and DE considered in the literature, which are frequently just linear in the DE density.

In fact, systems with nonlinear interaction are not, in general, analytically solvable. The case under consideration here is a rare exception. Notice that it is only in the limit $\rho_M \gg \rho_X$, equivalent to $\rho_M \approx \rho$, i.e. at high redshift that the interaction becomes approximately linear in ρ_X and approaches the type of coupling dealt with, e.g., in Gavela et al. (2010) and Salvatelli et al. (2013).

For a constant EoS parameter w the matter-energy balance in (12) can be integrated,

$$\rho_M = \rho_{M0}\,[1+z]^{3(1+w)+\xi}\left[\frac{1 + r_0\,(1+z)^{\xi}}{1+r}\right]^{-1-\frac{3w}{\xi}}, \tag{14}$$

where $z = \frac{1}{a} - 1$ is the redshift parameter. The total energy density becomes

$$\rho = \rho_0 a^{-3}\left(\frac{r_0 + a^{\xi}}{r_0 + 1}\right)^{-\frac{3w}{\xi}}, \qquad \rho_0 = \frac{r_0 + 1}{r_0}\rho_{M0}\,, \tag{15}$$

where ρ_0 is the present value of the energy density ρ. Restricting ourselves to a universe with spatially flat sections, we obtain the Hubble rate

$$H = H_0 a^{-\frac{3}{2}}\left(\frac{r_0 + a^{\xi}}{r_0 + 1}\right)^{-\frac{3w}{2\xi}} \tag{16}$$

and the deceleration parameter $q = -1 - \frac{\dot{H}}{H^2}$,

$$q = \frac{1}{2} + \frac{3}{2}\frac{w}{r_0 a^{-\xi} + 1}\,. \tag{17}$$

The present matter fraction Ω_{M0} of the Universe is related to the ratio r_0 by $\Omega_{M0} = r_0/(1 + r_0)$. For the special case $p_X = -\rho_X$ we have (in the background)

$$T^{ik}_X = -\rho_X g^{ik} \qquad \text{and} \qquad \dot{\rho}_X = -Q\,, \tag{18}$$

equivalent to a **time-varying** cosmological term.

4 PERTURBATION DYNAMICS

4.1 General setup

Let us denote first-order perturbations by a hat symbol. Assuming the equality of all four velocities in the background, $u^a_M = u^a_X = u^a$, it follows from $g_{ik}u^i_A u^k_A = -1$ that the perturbed time components of the four-velocities are equal as well, i.e., $\hat{u}_0 = \hat{u}^0 = \hat{u}^0_M = \hat{u}^0_X = \frac{1}{2}\hat{g}_{00}$. Because of this property, at first order, the expressions $\rho_{M,a}u^a_M$ and $\rho_{X,a}u^a_X$ in the energy balances (4) and (5), respectively, are

$$\widehat{(\rho_{M,a}u^a_M)} = \hat{\rho}_{M,a}u^a_M + \rho_{M,a}\hat{u}^a_M = \dot{\hat{\rho}}_M + \dot{\rho}_M\hat{u}^0 \tag{19}$$

and

$$\widehat{(\rho_{X,a}u^a_X)} = \hat{\rho}_{X,a}u^a_X + \rho_{X,a}\hat{u}^a_X = \dot{\hat{\rho}}_X + \dot{\rho}_X\hat{u}^0\,, \tag{20}$$

respectively. This implies that at first order

$$\rho_{M,a}u^a_M = \rho_{M,a}u^a \quad \text{and} \quad \rho_{X,a}u^a_X = \rho_{X,a}u^a \tag{21}$$

are valid. The timelike projections of the derivatives along the four velocities of the components coincide with the corresponding projections along the total four velocity. In other words, there is only one timelike derivative. Obviously, this is no longer valid at higher orders.

Combining the balances (4) and (5) with (21) it follows that, up to first order,

$$\frac{\xi}{3}\Theta = \Theta_M + \frac{u_{Ma}Q^a}{\rho_M} + \left[-\Theta_X\,(1+w) + \frac{u_{Xa}Q^a}{\rho_X}\right]. \tag{22}$$

In the background ($\Theta_M = \Theta_X = \Theta$ and $u_{Ma}Q^a = u_{Xa}Q^a = u_aQ^a = -Q$) we recover relation (13). Equation (22) will be crucial to determine the perturbed source in the following subsection.

In a next step we define the scalar velocity potentials v, v_M and v_X for the spatial velocity perturbations by (Greek indices run from 1 to 3)

$$\hat{u}_\alpha = v_{,\alpha}\,, \quad \hat{u}_{M\alpha} = v_{M,\alpha}\,, \quad \hat{u}_{X\alpha} = v_{X,\alpha}\,. \tag{23}$$

Directly from the definition of Θ it follows that

$$\hat{\Theta} = \frac{1}{a^2}\,(\Delta v + \Delta\chi) - 3\dot{\psi} - 3H\phi\,, \tag{24}$$

where Δ is the three-dimensional Laplacian and where we have introduced the line element for scalar perturbations,

$$\mathrm{d}s^2 = -\,(1+2\phi)\,\mathrm{d}t^2 + 2a^2F_{,\alpha}\mathrm{d}t\mathrm{d}x^\alpha + a^2\,[(1-2\psi)\,\delta_{\alpha\beta} + 2E_{,\alpha\beta}]\,\mathrm{d}x^\alpha\mathrm{d}x^\beta, \tag{25}$$

together with the abbreviation

$$\chi \equiv a^2\left(\dot{E} - F\right). \tag{26}$$

Via the variable F the spatial velocity components $\hat{u}^\mu$ are related to the potential v,

$$a^2\hat{u}^\mu + a^2F_{,\mu} = \hat{u}_\mu \equiv v_{,\mu}\,. \tag{27}$$

Analogous relations are valid for the velocity variables of the components. Similarly to (24) one has ($A = X, M$)

$$\hat{\Theta}_A = \frac{1}{a^2}\,(\Delta v_A + \Delta\chi) - 3\dot{\psi} - 3H\phi\,. \tag{28}$$

For the differences $\hat{\Theta}_A - \hat{\Theta}$ it follows that

$$\hat{\Theta}_A - \hat{\Theta} = \frac{1}{a^2}\,(\Delta v_A - \Delta v)\,. \tag{29}$$

According to the perfect-fluid structure of both the total energy-momentum tensor and the energy-momentum tensors of the components in (2), and with $u^a_M = u^a_X = u^a$ in the background, we have first-order energy-density perturbations $\hat{\rho} = \hat{\rho}_M + \hat{\rho}_X$, pressure perturbations $\hat{p} = \hat{p}_M + \hat{p}_X = \hat{p}_X$ and

$$\begin{aligned} \hat{T}^0_\alpha &= \hat{T}^0_{M\alpha} + \hat{T}^0_{X\alpha} \\ &\Rightarrow (\rho + p)\,\hat{u}_\alpha = \rho_M \hat{u}_{M\alpha} + (\rho_X + p_X)\,\hat{u}_{X\alpha}. \end{aligned} \tag{30}$$

With the definitions in (23) relation (30) implies

$$\begin{aligned} v_M - v &= (1+w)\,\frac{\rho_X}{\rho + p}\,(v_M - v_X)\ , \\ v_X - v &= -\frac{\rho_M}{\rho + p}\,(v_M - v_X)\ . \end{aligned} \tag{31}$$

4.2 The perturbed source term

From now on we shall restrict ourselves to the case $p_X = -\rho_X$, equivalent to an EoS parameter $w = -1$, i.e., to perturbed vacuum energy. The departure of the background dynamics from the ΛCDM model is then quantified by the difference of the parameter ξ from $\xi = 3$. Under this condition it follows from (30) that

$$\begin{aligned} p_X = -\rho_X \quad \Rightarrow \quad \rho + p = \rho_M \quad \Rightarrow \quad & \hat{u}_{M\alpha} = \hat{u}_\alpha \\ \Rightarrow \quad & v_M = v. \end{aligned} \tag{32}$$

Since the component M is supposed to describe matter, it is clear from (30) that the perturbed matter velocity $\hat{u}_{M\alpha}$ coincides with the total velocity perturbation $\hat{u}_\alpha$. With $u^n_M = u^n$ up to first order, the energy balance in (4) (correct up to first order) can be written as

$$\rho_{M,a} u^a = -\Theta \rho_M - u_a Q^a\,, \qquad (w = -1)\,. \tag{33}$$

On the other hand, the total energy balance (cf. (1)) is $\rho_{,a} u^a = -\Theta\,(\rho + p)$. For the difference we find

$$\dot{\rho} - \dot{\rho}_M \equiv (\rho - \rho_M)_{,a}\, u^a = u_a Q^a\ . \tag{34}$$

Since, at least up to linear order, $\rho - \rho_M = \rho_X$, Eq. (34) is equivalent (up to the first order) to

$$\dot{\rho}_X \equiv \rho_{X,a} u^a = u_a Q^a\,. \tag{35}$$

In zeroth order we consistently recover (18). The first order of Eq. (35) is

$$\dot{\hat{\rho}}_X + \dot{\rho}_X \hat{u}^0 = (u_a Q^a)\hat{}\ . \tag{36}$$

Notice that Eq. (36) results from a combination of the total energy conservation and the matter energy balance. It has to be consistent with the DE balance (5). At first order, the latter becomes

$$\dot{\hat{\rho}}_X + \dot{\rho}_X \hat{u}^0 = (u_{Xa} Q^a)\hat{}\ . \tag{37}$$

Consistency then requires that

$$(u_{Xa} Q^a)\hat{} = (u_a Q^a)\hat{}\ , \tag{38}$$

i.e., the projections of Q^a along u_{Xa} and along u_a coincide. Explicitly,

$$(u_a Q^a)\hat{} = (u_a u^a Q)\hat{} = -\hat{Q}\ . \tag{39}$$

Under the conditions (38) and (39) relation (22) becomes (for $w = -1$)

$$\frac{\xi}{3}\hat{\Theta} = \hat{\Theta}_M - \hat{Q}\frac{\rho}{\rho_M \rho_X} - Q\left(\frac{\rho}{\rho_M \rho_X}\right)\hat{}\ . \tag{40}$$

Solving for $\hat{Q}$ we find, after some transformation,

$$\hat{Q} = Q\left[\frac{\hat{\Theta}}{\Theta} + \delta_M\,(1 - r) + r\delta\right], \quad \delta \equiv \frac{\hat{\rho}}{\rho}, \quad \delta_M \equiv \frac{\hat{\rho}_M}{\rho_M}, \tag{41}$$

where Q is the background expression (13). Since the combination of interest will be $\hat{Q} - Q\delta_M$, it is useful to rewrite (41) as

$$\widehat{\left(\frac{Q}{\rho_M}\right)} = \frac{Q}{\rho_M}\left[\frac{\hat{\Theta}}{\Theta} - r\,(\delta_M - \delta)\right]. \tag{42}$$

With the perturbed source term explicitly known, we may now, in the following subsection, establish the basic set of perturbation equations.

4.3 Basic set of perturbation equations

To establish the basic set of perturbation equations it is convenient to introduce the gauge-invariant quantities

$$\begin{aligned} &\delta^c = \delta + \frac{\dot{\rho}}{\rho} v\,, \qquad \delta^c_M = \delta_M + \frac{\dot{\rho}_M}{\rho_M} v\,, \\ &\delta^c_X = \delta_X + \frac{\dot{\rho}_X}{\rho_M} v\,, \qquad \hat{p}^c_X = \hat{p}_X + \dot{p}_X v \end{aligned} \tag{43}$$

as well as

$$\hat{\Theta}^c = \hat{\Theta} + \dot{\Theta} v \qquad \text{and} \qquad \hat{Q}^c = \hat{Q} + \dot{Q} v. \tag{44}$$

The superscript c stands for comoving. All the symbols have their physical meaning on comoving hypersurfaces $v = 0$. In terms of these gauge-invariant variables the total energy and momentum conservations can be combined to yield (cf. (Hipólito-Ricaldi, Velten & Zimdahl 2009))

$$\dot{\delta}^c - \Theta\frac{p}{\rho}\delta^c + \hat{\Theta}^c\left(1 + \frac{p}{\rho}\right) = 0\,. \tag{45}$$

The energy-density perturbations are coupled to the perturbations of the expansion scalar which are determined by the Raychaudhuri equation. At first-order this equation becomes (cf. (Hipólito-Ricaldi, Velten & Zimdahl 2009))

$$\dot{\hat{\Theta}}^c + \frac{2}{3}\Theta\hat{\Theta}^c + 4\pi G\rho\delta^c + \frac{1}{a^2}\frac{\Delta\hat{p}^c_X}{\rho + p} = 0\,. \tag{46}$$

Combining Eqs. (45) and (46), changing to a as independent variable ($\delta' \equiv \frac{d\delta^c}{da}$) and transforming into the $k-$ space, the resulting equation for the total density perturbations is

$$\begin{aligned} &\delta^{c\prime\prime} + \left[\frac{3}{2} - \frac{15}{2}\frac{p}{\rho} + 3\frac{p'}{\rho'}\right]\frac{\delta^{c\prime}}{a} \\ &\quad - \left[\frac{3}{2} + 12\frac{p}{\rho} - \frac{9}{2}\frac{p^2}{\rho^2} - 9\frac{p'}{\rho'}\right]\frac{\delta^c}{a^2} + \frac{k^2}{a^2 H^2}\frac{\hat{p}^c_X}{\rho a^2} \quad = \quad 0. \end{aligned} \tag{47}$$

Because of the scale-dependent pressure perturbation term this is not a closed equation for δ^c. To clarify the role of this term in (47) we introduce the sound speed c_s in the rest-frame $v = 0$ by $\hat{p}^c_X = c_s^2 \hat{\rho}^c_X$. The sound speed is considered here as a free parameter. In an interacting two-component system the sound does not, in general, propagate with the adiabatic sound speed c_{ad}, given by $c^2_{ad} = \dot{p}/\dot{\rho}$. Then, the first-order energy balance for the matter component takes the form

$$\dot{\delta}^c_M + \hat{\Theta}^c + c_s^2 \frac{\dot{\rho}_M}{\rho_M}\frac{\rho_X}{\rho_M}\delta^c_X = \widehat{\left(\frac{Q}{\rho_M}\right)}^c , \tag{48}$$

where

$$\widehat{\left(\frac{Q}{\rho_M}\right)}^c = \frac{\hat{Q}^c}{\rho_M} - \frac{Q}{\rho_M}\delta^c_M = \frac{Q}{\rho_M}\left[\frac{\hat{\Theta}^c}{\Theta} - r\left(\delta^c_M - \delta^c\right)\right] . \tag{49}$$

Since $\hat{\rho}^c_X = \hat{\rho}^c - \hat{\rho}^c_M$, we realize that the pressure perturbations can be written as

$$\frac{\hat{p}^c_X}{\rho_M} = c_s^2 S_M , \qquad S_M \equiv D^c - \delta^c_M , \tag{50}$$

where we have introduced the fractional quantity

$$D^c \equiv \frac{\rho^c}{\rho + p} = \frac{1+r}{r}\delta^c \qquad \Leftrightarrow \qquad \delta^c = \frac{r}{1+r}D^c . \tag{51}$$

It becomes obvious that via (50) the dynamics of δ^c in (47) is coupled to $S_M = D^c - \delta^c_M$. To describe the dynamics of S_M we couple equations (45) and (48):

$$\dot{S}_M + \frac{Q}{\rho_M}D^c - \frac{\dot{\rho}_M}{\rho_M}\frac{\hat{p}^c_X}{\rho_M} = -\widehat{\left(\frac{Q}{\rho_M}\right)}^c , \tag{52}$$

with the right-hand side of this equation given by (49). Eliminating $\hat{\Theta}^c$ in the expression (49) with the help of (45) provides us with

$$\dot{S}_M + \frac{Q}{\rho_M}D^c + \left(\Theta - \frac{Q}{\rho_M}\right)\frac{\hat{p}^c_X}{\rho_M} = \frac{Q}{\Theta\rho_M}\left[\dot{D}^c + \left(\frac{Q}{\rho_M} + \Theta\frac{r}{1+r}\right)D^c - \Theta r\, S_M\right] . \tag{53}$$

After some transformations the final equation for S_M is

$$S^{c\prime}_M + \frac{3}{1+r}\left[\left(\frac{\xi}{3} + r\right)c_s^2 - r\left(\frac{\xi}{3} - 1\right)\right]\frac{S^c_M}{a} = \left(1 - \frac{\xi}{3}\right)\frac{\delta^{c\prime}}{r}. \tag{54}$$

Equation (54) is coupled to the equation (47) for δ^c, which together with (50) becomes

$$\delta^{c\prime\prime} + \left[\frac{3}{2} - \frac{15}{2}\frac{p}{\rho} + 3\frac{p^\prime}{\rho^\prime}\right]\frac{\delta^{c\prime}}{a} - \left[\frac{3}{2} + 12\frac{p}{\rho} - \frac{9}{2}\frac{p^2}{\rho^2} - 9\frac{p^\prime}{\rho^\prime}\right]\frac{\delta^c}{a^2} + \frac{k^2}{a^2H^2}c_s^2\frac{r}{1+r}\frac{S^c_M}{a^2} = 0. \tag{55}$$

The coupled set of equations (54) and (55) is the main result of this paper. The explicit structure of the coefficients is

$$\frac{p}{\rho} = -\frac{1}{1 + r_0 a^{-\xi}} , \quad \frac{p^\prime}{\rho^\prime} = \frac{\frac{\xi}{3} - 1}{1 + r_0 a^{-\xi}} , \quad H = H_0 a^{-\frac{3}{2}}\left(\frac{r_0 + a^\xi}{r_0 + 1}\right)^{\frac{3}{2\xi}} . \tag{56}$$

The total EoS parameter approaches zero at high redshifts. The adiabatic sound speed square is positive for $\xi > 3$ and it is negative for $\xi < 3$. For $\xi = 3$ one consistently recovers the ΛCDM model with $\frac{p^\prime}{\rho^\prime} = Q = 0$. Only if the pressure perturbations of the dark energy are negligible, the equation for δ^c decouples from that for S^c_M.

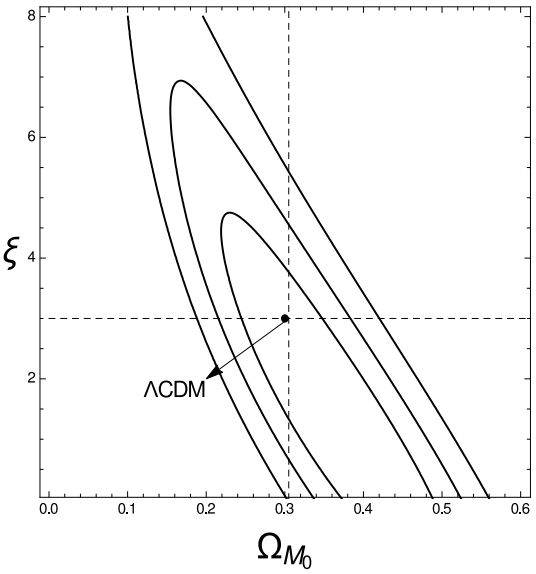

Figure 1. Two-dimensional contour lines (1σ, 2σ and 3σ CL) in the Ω_{M0}-ξ plane, based on the JLA data set. The point with the best-fit values $\Omega_{M0} = 0.30^{+0.04}_{-0.05}$ and $\xi = 2.99^{+0.90}_{-1.45}$ for the scaling model is almost indistinguishable from the point that characterizes the ΛCDM model.

4.4 Matter perturbations

The set (54) and (55) for S^c_M and δ^c, respectively, describes the entire perturbation dynamics of the system. With this system solved, the matter perturbations δ^c_M are then obtained as the combination

$$\delta^c_M = \frac{1+r}{r}\delta^c - S^c_M . \tag{57}$$

To evaluate the set (54) and (55) we have to consider its behavior in the high-redshift limit. Since $r \gg 1$ for $a \ll 1$ one has

$$\frac{p}{\rho} \ll 1 , \qquad \frac{p^\prime}{\rho^\prime} \ll 1 , \quad a^2H^2 \gg H_0^2 \qquad (a \ll 1) . \tag{58}$$

Under this condition Eq. (55) reduces to

$$\delta^{c\prime\prime} + \frac{3}{2}\frac{\delta^{c\prime}}{a} - \frac{3}{2}\frac{\delta^c}{a^2} = 0 \qquad (a \ll 1) , \tag{59}$$

which coincides with the corresponding equation for the Einstein-de Sitter universe. It has the growing solution $\delta^c = c_1 a$ where c_1 is a constant. Equation (54) also decouples and reduces to

$$S^{c\prime}_M + \left(3 - \xi + 3c_s^2\right)\frac{S^c_M}{a} = 0 \qquad (a \ll 1) . \tag{60}$$

It has the solution

$$S^c_M \propto a^{-\left(3-\xi+3c_s^2\right)} \qquad (a \ll 1) , \tag{61}$$

which is constant exactly only in the ΛCDM limit $\xi = 3$ and $c_s^2 = 0$. It decays for $\xi < 3(1 + c_s^2)$. For the matter perturbations at $a \ll 1$ this implies

$$\delta^c_M \approx \delta^c \qquad (a \ll 1) \tag{62}$$

as expected for $r \gg 1$.

For $\xi > 3(1 + c_s^2)$ the quantity S^c_M may also grow. But as long as it remains close to $\xi = 3$ the growth will be weaker than the growth of δ^c and (62) is still valid.

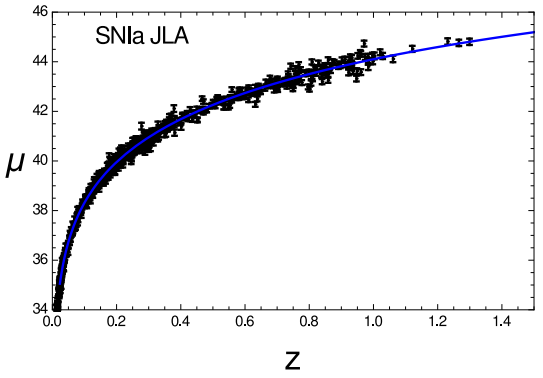

Figure 2. Redshift dependence of the best-fit luminosity-distance modulus of our model compared with the data from the JLA sample.

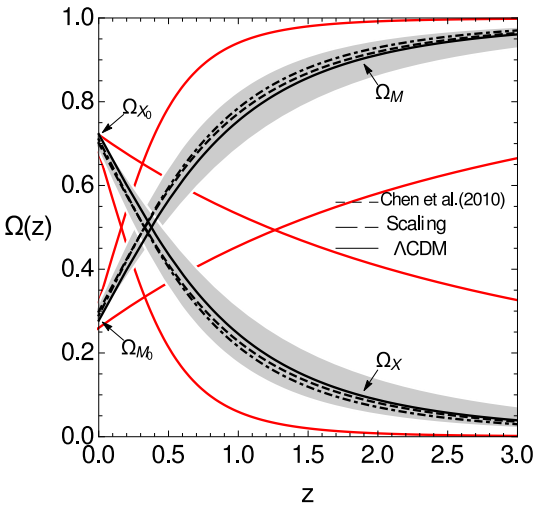

Figure 3. Fractional densities of DE and DM as functions of the redshift. The dot-dashed curves represent the best-fit values found in Chen et al. (2010), dashed curves correspond to the best-fit values of our model based on the JLA sample and continuous curves denote the ΛCDM model. The red lines confine the 1σ CL region of Chen et al. (2010), the gray area represents that of our analysis.

5 COMPARISON WITH OBSERVATIONAL, RESULTS AND DISCUSSIONS

Now we look for observational consequences of the model based on the ansatz (10) both for the homogeneous background dynamics and for structure formation. Since any deviation from the standard model is accompanied by a non-gravitational coupling between DE and DM this amounts to check the viability of the existence of such type of interaction in the dark sector and to put limits on its strength.

As a first step we shall perform a χ^2-statistics both for the SNIa and for the LSS data in order to know, how the model is situated in the observational branch. The χ^2-statistics is based on the expression

$$\chi^2(\theta) = \Delta y(\theta)^T \mathbf{C}^{-1} \Delta y(\theta) \tag{63}$$

with $\Delta y(\theta) = y_i - y(x_i;\theta)$ and the covariance matrix $\mathbf{C}$ of data y_i. The quantities y_i represent the observational data (in our case SNIa or LSS) which are compared with the theoretical predictions $y(x_i|\theta)$ with a set of parameters θ. Since we will consider the data as Gaussianly distributed the likelihood $\mathcal{L}$ is related to χ^2 by $\mathcal{L} \propto \exp\left(-\frac{\chi^2(\theta)}{2}\right)$.

Let us start with the 740 data points of the JLA sample (Betoule et al. 2014). This updates a previous analysis in Chen et al. (2010) based on the Constitution data set (Hicken et al. 2009). In this case y represents the luminosity-distance modulus, which is theoretically calculated as

$$\mu = 5 \log d_L(z) + \mu_0 \,, \tag{64}$$

with $\mu_0 = 42,384 - 5\log h$, where

$$d_L = (z+1)\, H_0 \int_0^z \frac{dz'}{H(z')} \,, \tag{65}$$

and h is defined by $H_0 = 100h\mathrm{kms}^{-1}\mathrm{Mpc}^{-1}$. The Hubble rate $H(z)$ is given by eq. (16) with a replaced by $a = (1+z)^{-1}$. Observational data points of the luminosity-distance modulus were calculated using the relation (Betoule et al. 2014)

$$\mu_{obs} = m_B^* - (M_B - \alpha X_1 + \beta C) \,, \tag{66}$$

where m_B^* corresponds to the observed peak magnitude in rest frame B band and α, β and M_B are nuisance parameters, X_1 is related to the time stretching of the light-curves, and C corrects the color at maximum brightness. In order to calculate completely μ_{obs} and its covariance matrix we followed the steps suggested in Betoule et al. (2014) and used the JLA data [1].

In the most general case there are four free parameters: $\theta = (h, \Omega_{M0}, \xi, w)$. Then, marginalizing over h and minimizing the χ^2-function we could find the best-fit values for the three remaining free parameters. However, the results based on the JLA data indicate an EoS parameter very close to $w = -1$. Moreover, our perturbation analysis was performed for this case as well and thus hereinafter we will use $w = -1$. Then we are left with the parameters ξ and Ω_{M0}. On this basis we find the two-dimensional curves in the $\Omega_{M0} - \xi$ plane shown in Fig. 1. The continuous curves represent the confidence levels (CL) at 1σ, 2σ and 3σ. The point characterizes the best-fit values for our scaling model. It is almost indistinguishable from the point of best-fit values for the ΛCDM model. Note that the values for ξ are highly degenerate. The curve in Fig. 2 shows the redshift dependence of the best-fit luminosity-distance modulus of our model compared with the data from the JLA sample.

In order to illustrate the consequences of the best-fit values of the model for the background dynamics, we plot the fractional densities of DE and DM and of the deceleration parameter as functions of the redshift in Figures 3 and 4, respectively. In these figures we also included the results of a previous analysis in Chen et al. (2010) (dot-dashed curves in Fig. 3 and blue curve in Fig. 4). The dashed curves represent the best-fit values for our model, the solid curves those for the ΛCDM model. The red lines confine the 1σ CL region of Chen et al. (2010), the gray area represents that of our analysis. The error for the best-fit value of Ω_M is reduced by approximately 25%, the error of the best-fit ξ value by approximately 73% in relation to Chen et al. (2010). Com-

[1] http://supernovae.in2p3.fr/sdss_snls_jla/ReadMe.html

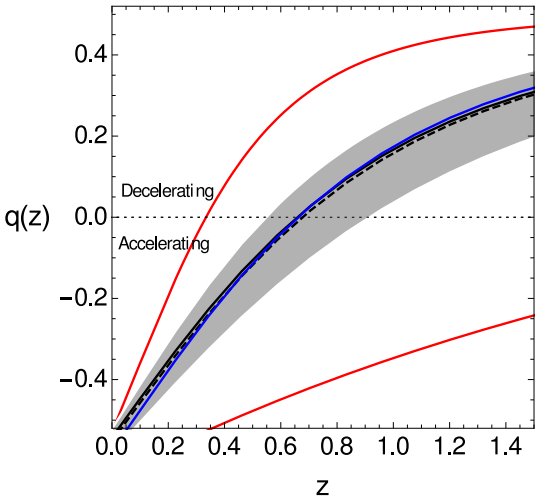

Figure 4. Deceleration parameter as function of the redshift. The blue curve represents the best-fit values in Chen et al. (2010), the dashed curve corresponds to the best-fit values of our model for the JLA sample and the continuous curve characterizes the ΛCDM model. The red lines confine the 1σ CL region of Chen et al. (2010), the gray area represents that of our analysis.

pared with the use of the Union 2.1 sample (Suzuki et al. 2012), the error of Ω_M is reduced by about 5% and the error of ξ by about 39%. Note that the behavior of the scaling model is practically the same as that of the ΛCDM model, i.e., the current SNIa samples can not discriminate between these models. The same indistinguishability happens for the deceleration parameter as seen in Fig. 4 where we plotted $q(z)$ for our model, for the model in Chen et al. (2010) and for the ΛCDM model. Again, the gray color indicates the region at 1σ CL.

Now let us perform an analysis of the perturbation dynamics. Here we have the sound speed square c_S^2 as an additional parameter. To get an idea of the role of this parameter we solved the system (54) and (55) for different values of c_S^2 with initial conditions provided by the limits of the model for $a << 1$. In this limit eq. (55) reduces to eq. (59), while the initial condition for eq. (54) is found from eq. (61) which governs the evolution of S_M at early times. This procedure to choose initial conditions is similar to that described in more detail in Fabris, Shapiro & Solá (2007); Hipólito-Ricaldi, Velten & Zimdahl (2010). The results for the integration of the system (54)-(55) for a typical case, we have chosen here $\Omega_{M0} = 0.275$ and $\xi = 2.99$, are shown in Fig. 5 which visualizes the evolution of total density contrast, the relative density contrast and the matter density contrast as functions of the scale factor for three different scales. Figures 5a, 5b and 5c present the curves for $k = 45\,hMpc^{-1}$, figures 5d, 5e and 5f those for $k = 10\ h\mathrm{Mpc}^{-1}$ and figures 5g, 5h and 5i those for $k = 0.3\ h\mathrm{Mpc}^{-1}$. Similar plots can be obtained for different values of Ω_{M0} and ξ.

Several features of Fig. 5 are worth discussing. For example, according eq. (61) the initial conditions for S_M depend on the sound velocity square c_S^2. However, the behavior of S_M is similar for all the cases in Fig. 5. It has constant values (or almost constant values for $k = 0.3\ h\mathrm{Mpc}^{-1}$) in early times and starts oscillating between $a \approx 0.08$ and $a \approx 0.12$. The amplitude of these oscillations is small and contributes only marginally to the matter density contrast δ_M (see eq. (57)). Thus, δ and δ_M (we have omitted the superscripts c in this figure) show a very similar behavior, i.e., relation (62) remains approximately valid. The evolution of both the total density contrast δ and of the matter density contrast δ_M depends crucially on c_S^2. Our calculations show that for higher values of the sound velocity square c_S^2 there appear oscillations both in δ and in δ_M at about $a \approx 0.1 - 0.2$. At values of c_S^2 lower than a threshold value c_{S0}^2, i.e., for $c_S^2 < c_{S0}^2$ the oscillations disappear. We confirmed numerically that c_{S0}^2 is inversely proportional to k. For example, for $k = 45\ h\mathrm{Mpc}^{-1}$ we have $c_{S0}^2 = 1.7 \times 10^{-4}$ (see figures 5a, 5b and 5c), for $k = 10\ h\mathrm{Mpc}^{-1}$ the threshold changes to $c_{S0}^2 = 1.8 \times 10^{-2}$ (see figures 5d, 5e and 5f) and for $k = 0.3\ h\mathrm{Mpc}^{-1}$ the threshold value is $c_{S0}^2 = 3.2 \times 10^{-1}$ (see figures 5g, 5h and 5i).

Since with the solution of our basic system the matter density contrast $\delta_M(a)$ is known according to relation (57), we can construct the matter power spectrum (P_k) and study the influence of c_S^2 on this spectrum. In Fig. 6 we show the matter power spectrum for different values of the sound velocity. As to be expected, also the spectrum exhibits oscillations for larger values of c_S^2. Such type of behavior is similar to what is known from unified models of the dark sector, notably from Chaplygin-gas models. Since oscillations of the matter distribution are not observed, those models have temporarily fallen out of favor (Sandvik et al. 2004). However, non-adiabatic pressure perturbations may reduce the effective sound speed to very small values which may cure the problem of oscillations (Hipólito-Ricaldi, Velten & Zimdahl 2009; Borges et al. 2013). As a consequence, unified models continue to be discussed as potential alternatives to the ΛCDM model. In our case c_S^2 is a free parameter and we shall discard models for which c_S^2 is larger than the mentioned threshold value c_{S0}^2.

Now, the y_i in the expression (63) represent the LSS DR9 data (Ahn et al. 2012), while y is the theoretically calculated matter power spectrum P_k. The set of free parameters is $\theta = (c_S^2, \Omega_{M0}, \xi)$. We have used the publicly available DR9 data covariance matrix and restricted the wavenumber to the range $0.002h\mathrm{Mpc}^{-1} < k < 0.2h\mathrm{Mpc}^{-1}$ for which a linear approximation seems appropriate.

To avoid the mentioned unwanted and non-observed oscillations very small values of c_S^2 are required. For our calculations we take $c_S^2 \sim 10^{-4}$. Such value will ensure the absence of oscillations until $k \sim 45\,h\mathrm{Mpc}^{-1}$, equivalent to a scale of $\sim 0.02\,h^{-1}\mathrm{Mpc}$. Hence, we continue our analysis with only two free parameters, namely Ω_{M0} and ξ. Minimizing the χ^2-function under this condition we find the best-fit values visualized in the Ω_{M0}-ξ plane of Fig. 7. The continuous contour lines represent the 1σ and 2σ confidence levels. We performed also a joint analysis by using the combined SNIa + LSS data where $\chi^2 = \chi^2_{SNIa} + \chi^2_{LSS}$. The results are presented in Fig. 7 as well, where the grey color represents the region between the 1σ and 2σ CLs. The best-fit values for the combined analysis are summarized in Table 1. There is a tendency for $\xi > 3$, i.e., for an energy transfer from DM to DE. While the JLA data alone show a big degeneracy, the latter is largely removed by the large-scale-structure data. In Fig. 8 we present four different curves. Curve 1 is the

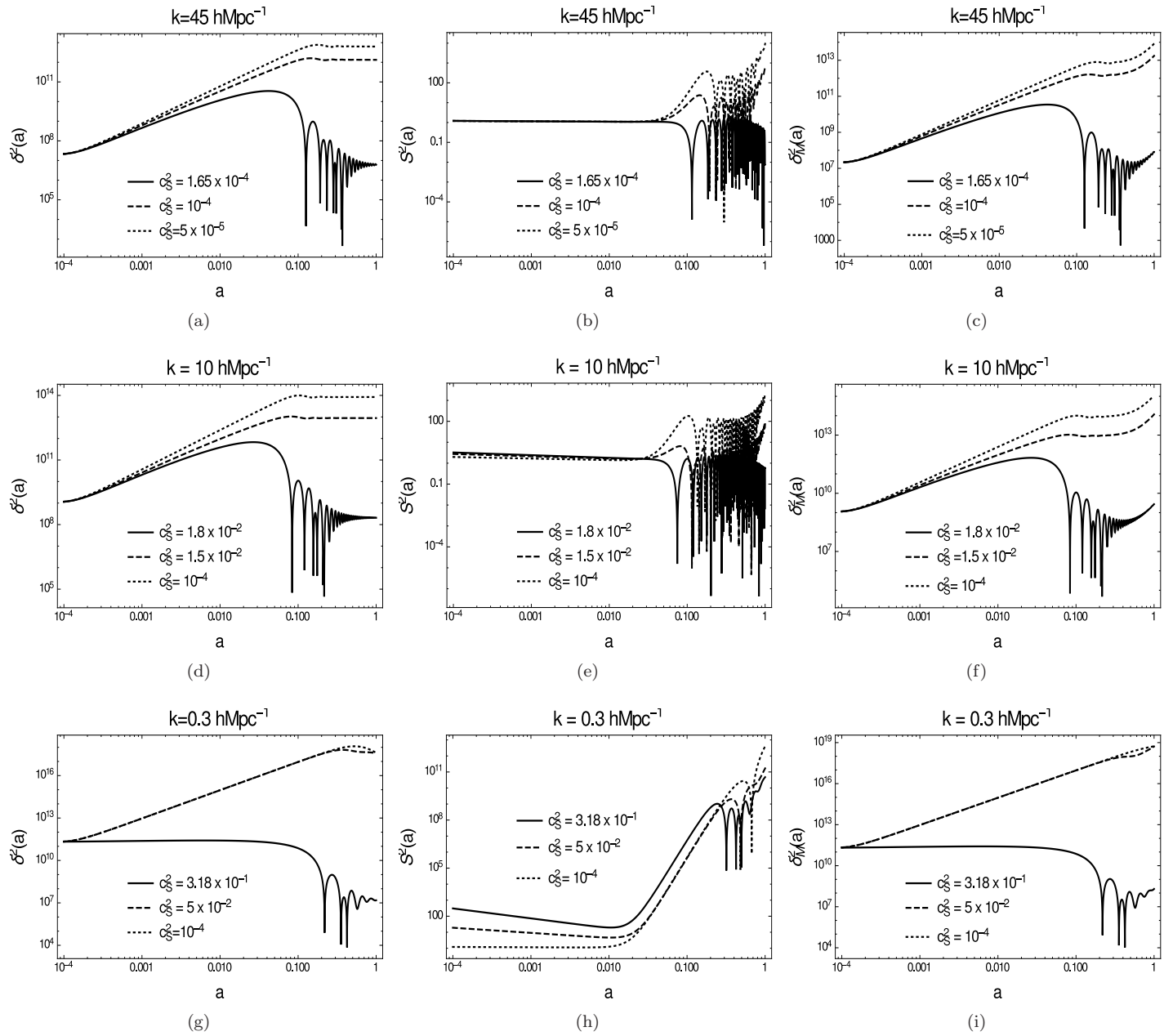

Figure 5. Total density contrast δ, relative density contrast S_M and matter density contrast δ_M as functions of the scale factor for three different scales. Figures 5a, 5b and 5c represent the curves for $k = 45\ h\mathrm{Mpc}^{-1}$, figures 5d, 5e and 5f those for $k = 10\ h\mathrm{Mpc}^{-1}$ and figures 5g, 5h and 5i those for $k = 0.3\,h\mathrm{Mpc}^{-1}$. We have assumed here $\Omega_{M0} = 0.275$ and $\xi = 2.99$. In all cases high values of the sound speed lead to oscillations while smaller values do not. (Note that we have omitted here the superscripts c.)

best-fit model for the DR9 data set. It has $\Omega_m \sim 0.27$, $\xi \sim 3.26$ and $\chi^2_{\nu,DR9} = 1.20$. Curve 2 represents the best-fit model for the combined DR9+JLA data. The best-fit values are $\Omega_m \sim 0.27$, $\xi \sim 3.25$ and $\chi^2_{\nu,DR9+JLA} = 1.16$. Note that curve 1 and curve 2 are indistinguishable. To countercheck these results we have also chosen two parameter combinations from outside the 2CL solid contour: curve 3 is based on $\Omega_m \sim 0.30$ and $\xi \sim 3.8$ and has a $\chi^2_{\nu,DR9+JLA} = 2.14$ for the joint DR9+JLA data. The same model has a $\chi^2_{\nu,DR9} = 2.68$ when only DR9 data are considered. Curve 4 is constructed with $\Omega_m \sim 0.23$ and $\xi \sim 2.85$ and has a $\chi^2_{\nu,DR9+JLA} = 2.49$ when the combined DR9+JLA data sets are used. For DR9 data only one has $\chi^2_{\nu,DR9} = 3.09$. The fit to these values outside the 2σ contour is indeed considerably worse which supports our analysis.

Finally, with the known best-fit values we can infer the upper and lower bounds for the interaction strength. These values are presented in the outer right column of Table 1. As already mentioned, there is a tendency to values $\xi > 3$ which corresponds to $Q < 0$, equivalent to a transfer of energy from DM to DE. Qualitatively, this is in accordance with the results in Gavela et al. (2010) and Salvatelli et al. (2013) which are based on an interaction linear in the DE energy

Table 1. Best-fit values for the different tests of the scaling model with errors at 1σ CL. The source term Q is given in units of $H_0^3/8\pi G$.

Data	Ω_{M0}	ξ	χ^2_ν	Q
JLA	$0.30^{+0.04}_{-0.05}$	$2.99^{+0.90}_{-1.45}$	1.18	$+0.01^{+0.97}_{-0.61}$
DR9	$0.27^{+0.02}_{-0.01}$	$3.26^{+0.16}_{-0.16}$	1.20	$-0.15^{+0.09}_{-0.11}$
DR9+JLA	$0.27^{+0.01}_{-0.01}$	$3.25^{+0.15}_{-0.15}$	1.16	$-0.15^{+0.09}_{-0.09}$

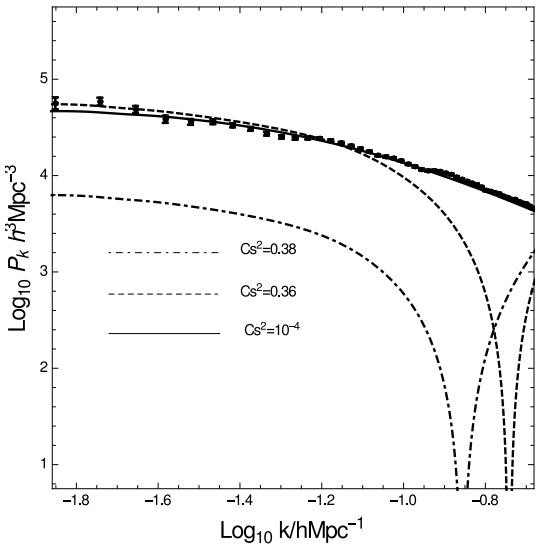

Figure 6. Matter power spectrum for different values of the sound velocity. There are oscillations for large values of c_S^2 but not for smaller values.

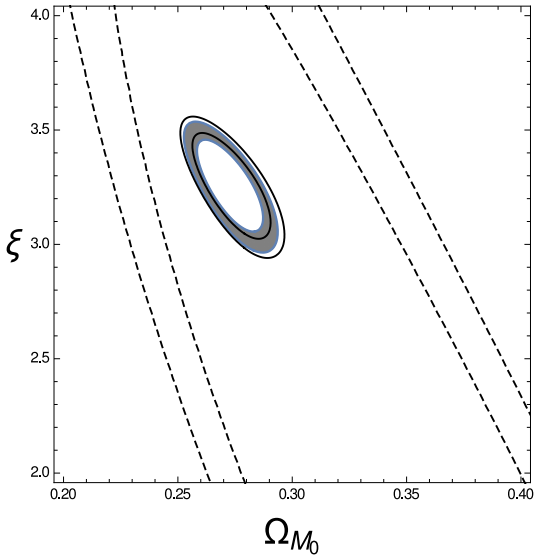

Figure 7. Ω_{M0}-ξ plane for the scaling model. Continuous contour lines represent the 1σ and 2σ CL based on the DR9 data sample. For comparison we have also included the results for the JLA sample (dashed lines). The grey region represents the 1σ and 2σ CL for the joint analysis JLA+DR9.

density. On the other hand, thermodynamic considerations prefer Q to be positive (Pavón & Wang 2009).

6 CONCLUSIONS

With the intention to quantify and, possibly, to soften the coincidence problem, Dalal et al. (2001) introduced a phenomenological parameter ξ that governs the dynamics of the ratio of the energy densities of DM and DE. Independently of whether one takes the coincidence problem seriously, the resulting cosmological dynamics represents a simple, testable modification of the standard model.

Starting point of this approach is not, as usual, an expression for the interaction between DM and DE but the mentioned dynamics of the energy-density ratio which can be compared with that of the ΛCDM model in a transparent manner. Any deviation from the standard dynamics is then traced back to a specific coupling between DM and DE. Different from most models discussed so far, this coupling is nonlinear, i.e., the interaction quantity Q contains a product of the energy densities of DM and DE. Most other interacting models are just linear in the DE density. For $\xi = 3$ and $w = -1$ the ΛCDM model is recovered. Any combination $w+\xi/3 \neq 0$ corresponds to a non-gravitational interaction between DM and DE. Any value $\xi < 3$ is considered to make the coincidence problem less severe. This model was tested against observational data in (Chen et al. 2010; Pavón, Sen & Zimdahl 2004; Dalal et al. 2001; Castro et al. 2012). However, in its original form and in the studies so far its validity is restricted to the homogeneous and isotropic background dynamics. Here we generalized this model to enable a study of the perturbation dynamics as well. To this purpose we replaced the scale factor in the model defining relation by a more general covariantly defined length scale which reduces to the scale factor in the appropriate limit. We performed a gauge-invariant first-order perturbation analysis which enabled us to obtain the fractional matter density perturbations as a combination from a coupled system of equations for the total and relative perturbations. Like in other DE models, the effective non-adiabatic sound velocity has to be smaller than a certain threshold value to avoid (unobserved) oscillations in the matter perturbations. Within a χ^2 analysis and focusing on the case of perturbed vacuum energy $w = -1$, the resulting matter power spectrum was confronted with data from the SDSS DR9 survey. We studied the dependence of the power spectrum on the values of the parameter ξ. The results for the background dynamics were improved considerably compared with a previous study. Using the JLA data alone results in a large degeneracy in the Ω_{M0}-ξ plane which does not allow for a definite conclusion concerning the sign of the interaction. This degeneracy is substantially reduced by the DR9 large-scale-structure data which prefer $\xi \approx 3.25$. This corresponds to an energy transfer from DM to DE. The ΛCDM model with

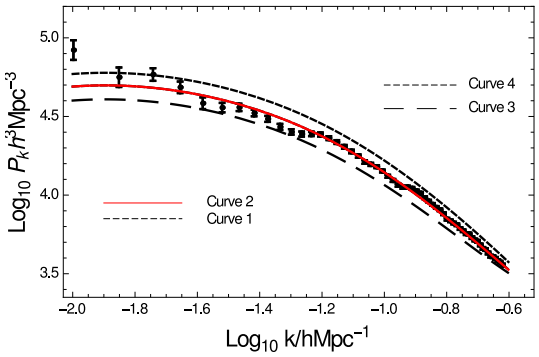

Figure 8. Matter power spectrum with $\Omega_{M0} = 0.27$ for several values of ξ, including the best-fit value, for the DR9 data.

$\xi = 3$ is compatible with our analysis at the 2σ confidence level.

Finally we remark that for a more realistic study of matter clustering on smaller scales in the presence of DE and for a better understanding of the role of c_S^2 in structure formation a nonlinear treatment is necessary. Processes as virialization and spherical collapse which were outside the scope of the present paper have necessarily to be considered. We hope to come back to this in future work. Further constraints on our nonlinear model are expected from CMB data. This is currently under investigation.

ACKNOWLEDGMENTS

ARF acknowledges support from CAPES (Brazil). WSHR is thankful to FAPES by the grant (BPC No 476/2013) under which this work was carried out. WZ was supported by CNPq and FAPES. We thank the anonymous referee for constructive suggestions.

REFERENCES

Ahn C. P. et al., 2012, ApJS, 203, 21.
Alcaniz J.S., Maia J. M. F., 2003, Phys. Rev. D, 67, 043502.
Aldrovandi R., Beltrán Almeida J. P., , Pereira J. G., 2005, Grav. & Cosmol., 11, 277.
Al-Rawaf A. S., 2001, Mod. Phys. Lett. A, 14, 633.
Arbab A. I., Abdel-Rahman A. M. M., 1994, Phys. Rev. D, 50, 7725.
Barrow J. D. , Clifton T. , 2006, Phys. Rev. D,73, 103520.
Bauer F., 2005, Class. Quant. Grav. 22, 3533.
Berman M. S., 1991, Phys. Rev. D, 43, 1075.
Bertolami O., 1986, Nuovo Cimento Soc. Ital. Fis., 93, 36.
Bertolami O., Martins P. J., 2000, Phys. Rev. D, 61, 064007.
Borges H. A. , Carneiro S., Fabris J. C., Zimdahl W., 2013, Phys. Lett. B, 727, 37.
Betoule M. et. al., 2014, Astron.Astrophys., 568, A22.
Castro D.R., Velten H.E.S., Zimdahl W., 2012, JCAP, 1206, 024.
Carvalho J. C., Lima J. A. S., Waga I., 1992, Phys. Rev. D, 46, 2404.
Chen W. , Wu Y-S., 1990, Phys. Rev. D, 41, 695.
Chen Y., Zhu Z.-H., Alcaniz J.S. and Gong Y., 2010, ApJ, 711, 439.
Cunha J. V., Santos R. C., 2004, IJMP D, 13, 1321.
Dalal N., Abazajian K., Jenkins E., Manohar A.V., 2001, Phys. Rev. Lett., 86, 1939.
Ellis G.F.R., 2009, Gen.Relativ.Grav., 41, 581. (reprint of G.F.R. Ellis in: R.K. Sachs (ed.), Proceedings of the International School of Physics "Enrico Fermi", Course 47: General relativity and cosmology, pp. 104 - 182. Academic Press, New York and London (1971).)
Elizalde E., Nojiri S. , Odintsov S. D. , Wang P., 2005, Phys. Rev. D, 71, 103504.
Fabris J.C. , Shapiro I.L., Solá J. , 2007, JCAP, 0702, 016.
Freese K., Adams F.C., Frieman J.A., Mottola E., 1987, Nucl. Phys.B, 287, 797.
Gavela M.B., Lopez Honorez L., Mena O., Rigolin S., 2010, JCAP, 1011, 044.
Hicken M. et. al., 2009, ApJ, 700, 1097.
Hipólito-Ricaldi W.S. , Velten H.E.S., Zimdahl W., 2009, JCAP, 0906, 016.
Hipólito-Ricaldi W.S. , Velten H.E.S., Zimdahl W., 2010, Phys. Rev. D, 82, 063507.
Horvat R., 2004, Phys. Rev. D, 70, 087301.
John M. V., Joseph K.B. , 2000, Phys. Rev. D, 61, 087304.
Lima J. A. S., Trodden M. , 1996, Phys. Rev. D, 53, 4280.
Mak M. K., Belinchón J. A., Harko T., 2002, IJMP D, 11, 1265.
Mbonye M. R., 2003, IJMP A, 18, 811.
Montenegro Jr. A. E., Carneiro S. , 2007, Class. Quant. Grav., 24, 313.
Opher R., Pelinson A., 2004, Phys. Rev. D, 70, 063529.
Overduin J. M. , 1999, ApJ. 517, L1.
Overduin J. M., Cooperstock F. I., 1998, Phys. Rev. D, 58, 043506.
Özer M. , Taha M. O., 1986, Phys. Lett. B, 171, 363.
Özer M., Taha M. O., 1987, Nucl. Phys. B , 287, 776.
Park C.-G. , Hwang J. , Lee J. , Noh H., 2009, Phys. Rev. Lett. ,103, 151303.
Pavón D., Sen S., Zimdahl W., 2004, JCAP, 0405, 009.
Pavón D., Wang B., 2009, Gen.Rel.Grav., 41, 1.
Pettorino V., 2013, Phys. Rev. D, 88, 063519.
Salvatelli V., Marchini A., Lopez-Honorez L., Mena O. 2013, Phys. Rev. D, 88, 023531.
Sandvik H.B., Tegmark M., Zaldariaga M., Waga I., 2004, Phys. Rev. D, 69, 123524.
Shapiro I. L., Solà J., España-Boatenet C., Ruiz-Lapuente P., 2003, Phys. Lett. B, 574, 149.
Shapiro I. L., Solà J., Štefančic H., 2005, JCAP, 0501, 012.
Suzuki N. et al., 2012,ApJ., 746, 85.
Vishwakarma R. G., 2001, Gen. Rel. Grav., 33, 1973.
Wang P., Meng X., 2005, Class. Quant. Grav., 22, 283.
Wang B., Gong Y. , Abdalla E. , 2005, Phys. Lett. B, 624, 141.
Wang B., Lin C.Y., Abdalla E., 2006, Phys. Lett. B, 637, 357.
Zimdahl W., Pavón D., 2003, Gen.Rel.Grav., 35, 413.